Removing Phosphate From Aquatic Environments Utilizing Fe-Co/Chitosan Modified Nanoparticles

Tadeh Issaian[a*]

Julia Constanza Reyes Cuellar[a]

Abstract:

Chitosan modified iron-cobalt nanoparticles (CMNPs) were used for phosphate adsorption in synthetic wastewater and river water from the Jordan river in Tunja, Boyacá, Colombia. Phosphate adsorption by CMNPs reached 52.7% in synthetic wastewater and 58.7% in water taken from the Jordan river. This indicates that the CMNPs ability to adsorb phosphates is independent of other components within river water. Additionally, adsorption measurements were taken using the average pH, temperature, and phosphate concentration of the river water in order to ensure results comparable to those of (Kim 2017). A maximum adsorption rate of 0.138 mg of phosphate per gram of adsorbent was found with the majority of adsorption taking place within the first 15 minutes of contact with the adsorbent. The adsorption of phosphates using CMNPs presents an effective and environmentally friendly solution to reducing phosphates in aquatic ecosystems without altering the characteristics of river water.

Key Words: Chitosan, Iron-Cobalt Nanoparticles, Phosphate Adsorption, Wastewater Treatment

1. INTRODUCTION:

Phosphorus plays a key role in cellular mechanisms and ecosystems, including the ability of a cell to store and transfer energy, as well as in its genetic makeup. Cells utilize adenosine triphosphate (ATP) as energy storage for muscle contraction, photosynthesis, and protein synthesis. [1] [2] Phosphorus is typically found in rocks and mineral deposits, although, it is considered to be a limited resource. [3] Through erosion and human activities, phosphate ions are gradually released, and their solubility in water presents problems for aquatic ecosystems. Phosphate exists primarily in two forms: orthophosphate and elemental phosphorus. [4] Orthophosphate is the primary form of dissolved phosphate in aquatic environments, however depending on environmental conditions, particular phosphates may also cycle from one form to the other. [4] One of the problems that high phosphate concentrations in aquatic ecosystems cause is eutrophication.

Eutrophication is increased plant or algae growth due to an increase in nutrients. [5] [6] An increase in concentration of nutrients causes plants and algae to grow depleting the water oxygen levels to a point at which few species can survive. Although typical phosphate concentrations in unpolluted freshwater systems can range from 0.01 mg/L to 0.025 mg/L, increases in agricultural activity and city wastewater can increase phosphate concentrations which may lead to eutrophication. [7]

The city of Tunja is located about 130 km northeast of Bogotá on the Andes mountain range and is the capital of the department of Boyacá, Colombia. Due to its geographical location, it is the source of the Jordan river which runs through the city of Tunja. At its source, the water looks crystal clear; however, as it flows through Tunja, it takes on a murky and pungent character which is due to industrial waste, rainfall runoff, and agricultural runoff. The regulatory agency in charge of monitoring the quality of the river found

---

[a]   Universidad Pedagógica y Tecnológica de Colombia.

[a]   Universidad Pedagógica y Tecnológica de Colombia.

elevated levels of phosphorus, with concentrations ranging between 0.801 and 11.0 mg/L, which are greater than the legally permitted concentration of 10.0 mg/L. [8]

In order to help mitigate the consequences of excess phosphorus concentrations, a combination of magnetic nanoparticles and polysaccharides (chitosan) are linked together to form chitosan modified nanoparticles (CMNPs). CMNPs were chosen due to previous studies demonstrating their ability to adsorb phosphates in aquatic environments. [9] [10] [11] [12] The nanoparticles synthesized utilize a Co/Fe molar ratio equal to 80/20 due to its superior magnetic properties which aide in its recuperation. [13] Chitosan, a polysaccharide which is derived from the shells of crustaceans, can adsorb various pollutants and is biodegradable. [9] Magnetic nanoparticles alone are unable to adsorb phosphates as they do not have the specific site nor charge; however, they are insoluble in water [14]. Chitosan has been broadly studied as composite for controlled release or adsorption of different metals or organic molecules [15] Modified chitosan can create bonds with dissolved phosphate, but as a result becomes soluble in water. When the nanoparticles and chitosan are combined, they form a gel, which has a low solubility in water and a greater affinity for adsorbing phosphates. [12]. This reduced solubility and ability to perform multiple adsorption/desorption cycles with great efficiency is a primary reason why it is of great interest. [9] [16] [10] [17] This makes it particularly useful to adsorb phosphates within an aquatic environment to reduce the likelihood of eutrophication.

2. MATERIALS AND METHODS

All the reagents utilized were of analytical grade. Iron sulfate heptahydrate 99.5%, cobalt sulfate heptahydrate 99.5%, sodium hydroxide 98%, acetic acid 99.5%, ammonium meta-vanadate 98%, ammonium molybdate 98%, ethylene glycol 99%, and methanol 99% were obtained from Panreac. Hydrochloric acid was obtained from J.T. Baker and monopotassium phosphate 99% was obtained from Lobachemie. All solutions were prepared using distilled water. Phosphate concentrations were determined using the Standard Methods (SM) protocol 4500 P-C utilizing vanadomolybdophosphoric acid and a Thermo Fisher

Scientific Genesys 10 UV-Vis spectrophotometer set at a wavelength of 420 nm. [18]

2.1 SYNTHESIS OF IRON-COBALT NANOPARTICLES

The method developed by Chirac (2008) was used to synthesize the magnetic nanoparticles. A stochiometric mix of iron (0.014M) and cobalt (0.057M) sulfides were dissolved in 50 mL of ethylene glycol. The pH was then adjusted to 11 using aqueous NaOH 3M and the entire mixture was refluxed for 4 h at a temperature of 185°C in order to obtain nanoparticles of $Co_{80}Fe_{20}$. After refluxing, the mixture was cooled to room temperature and centrifuged for 1 h at 4000 RPM in order to separate the nanoparticles from the ethylene glycol. The nanoparticles were then washed with distilled water and dried in an oven at 40°C for 24 h. Calcination of the nanoparticles was performed at 600°C for 2 h to improve their magnetic behavior.

2.2 MODIFICATION OF IRON-COBALT NANOPARTICLES WITH CHITOSAN

The chitosan solution was based on the procedure developed by Kim (2017). The chitosan solution was prepared using a concentration of 3% w/w low molecular weight chitosan dissolved in 70mL of diluted acetic acid (2%w/w). This solution was heated to 60°C and mixed at 500 RPM for 12 h in order to facilitate a homogeneous mixture. 30 mL of distilled water containing the nanoparticles (6%w/w) was then added to the chitosan mixture. Afterwards, 50mL of NaOH 0.2M in methanol was then added to the nanoparticle/chitosan solution at a rate of 4mL/min and left to mix for 12 h. The resulting gel was then washed with deionized water and centrifuged in order to be applied to wastewater samples and synthetic wastewater.

2.3 APPLICATION OF CHITOSAN MODIFIED NANOPARTICLES (CMNPs) TO SYNTHETIC AND NATURAL WASTEWATER.

In order to test the CMNPs ability to adsorb phosphates, a phosphate mixture of 2.00 mg/L (KH2PO4) and distilled water was used to mimic natural wastewater. [9] All testing was performed with water at room temperature (23°C) and a pH

of 7.5. This synthetic wastewater was placed into a 1L bottle and pumped through a Vera Varistaltic Pump Plus (0.4 flow speed, 40 mL/min) and into the bottom of an Büchner flask. Afterwards, 15 g of the CMNP gel was placed at the bottom of the Büchner flask and mixed with the synthetic wastewater with a magnetic stir bar spinning at 500RPM. Once the water overflowed through the hose barb of the Büchner flask, 40 mL was collected in a 50mL Falcon conical centrifuge tube. This tube was then marked in order to measure phosphate adsorption. The rest of the solution in the Büchner flask was poured into separate 50mL Falcon conical centrifuge tubes. The tubes were then centrifuged for 30 min at 4000 RPM. In order to measure phosphate adsorption from the marked tube, 25mL of solution was taken and placed in a 50 mL volumetric flask. Then, 10 mL of vanadomolybdophosphoric acid was added with distilled water being filled up to the 50 mL line. This method developed a yellow color from which absorbance could be measured using a spectrophotometer set to 420nm. [18] The supernatant (CMNP gel) from all of the tubes was then extracted and placed in a beaker with 100 mL of NaOH 5mM for 12 h stirring at 500 RPM in order to release the bound phosphates and recuperate the CMNPs for reuse. This process was repeated for each adsorption/desorption cycle as well as with the use of natural wastewater. Variables were also adjusted, as mentioned in Table 1 below, in order to test adsorption/desorption efficiency regarding the different variables.

2.4 Characterization of CMNPs

Table 1: Experimental conditions

Exp	Variables			
	Water Type	Flow Rate mL/min	Desorption Time h	Quantity of CMNPs g
1	Synthetic	40	12	15
2	River	40	12	15
3	River	40	12	22.5
4	River	20	12	15
5	River	40	6	15

Phosphate concentrations were measured using a Thermo Fisher Scientific Genesys 10 UV-Vis spectrophotometer set at a wavelength of 420nm. To determine the structure and functional groups present in the sample, FTIR-ATR was performed using a Shimadzu IRPrestige-21. Additionally, XRD was performed to determine the crystalline structure of the nanoparticles using a PanAlytical X'Pert PRO X-Ray diffractometer. SEM images were taken with a Zeiss Sigma FE-SEM coupled with EDX spectroscopy, while TEM images were taken with a JEOL USA JEM 1200X.

2.5 Adsorption Isotherm Modeling

In order to determine the CMNPs ability to adsorb phosphates, an adsorption isotherm model was needed. A series of batch tests in test tubes were conducted to obtain the experimental data needed. 0.5g of CMNPs were added to each of the six Erlenmeyer flasks of 150mL. 50 mL of phosphate solution with a different initial concentration of phosphate was added: (C_0 = 0.5, 1.0, 3.0, 6.0, 20.0, and 50.0 mg P/L) to each of the flasks. The solutions were shaken on a horizontal shaker for 6 h at 150 RPM and at a temperature of 23°C. Afterwards, 25mL of the phosphate solution was taken and placed in a 50 mL volumetric flask. Then, 10 mL of vanadomolybdophosphoric acid was added with distilled water being filled up to the 50 mL line. This method developed a yellow color from which absorbance could be measured using a spectrophotometer set to 420nm. [18] The amount of phosphate adsorbed at equilibrium (q_e, mg/g) was calculated by the following equation:

$$q = \frac{(C - C)}{m} \, x \, V$$

103

Where C_0 and C_e are the initial and equilibrium phosphate concentrations in (mg/L), respectively. V is the volume of the solution in (L), and m is the mass of the adsorbent in (g).

The experimental isotherm would then be analyzed with the Langmuir isotherm models. The Langmuir isotherm model assumes that adsorption can only occur at a specific number of sites and that the adsorbent layer is one molecule thick. [19] The non-linear Langmuir adsorption isotherm is demonstrated by the following equation:

$$ q = q \; K \; \frac{C}{1 + K \; C} $$

Where q_e is the adsorption capacity in (mg/g), and q_m (mg/g) and K_L (L/mg) are constants related to adsorption capacity and energy of adsorption, respectively. Additionally, an adsorption kinetics test using 2mg/L of phosphate solution and 15g of adsorbent in a 250mL flask was performed. Measurements were taken every five minutes and quantified using the vanadomolybdophosphoric acid mentioned above. The equation utilized the non-linear Langmuir adsorption isotherm equation due to the fact that the graph was non-linear.

3. RESULTS

3.1 PHOSPHATE ADSORPTION

Table 2: Results from experimental conditions during phosphate removal

Exp	% of Phosphate Removed (2.0 mg/L initial P concentration)					
	1st Cycle	2nd Cycle	3rd Cycle	4th Cycle	5th Cycle	6th Cycle
1	52.73	42.97	37.11	33.20	29.30	25.39
2	58.72	42.70	37.37	33.81	30.25	24.91
3	89.52	85.59	84.28	79.04	72.93	66.38
4	63.91	59.13	54.35	51.74	47.39	43.04
5	54.35	34.42	25.36	9.06	1.81	N/A

The efficiency of phosphate removal under various conditions in both synthetic and natural river water is shown in Table 2. The results indicated that both the synthetic water and river water were equally able to be treated with CMNPs. These results are promising as other studies have indicated high phosphate adsorption capabilities in low pH environments (pH of 3-8) and with a significantly slower flow rate (7 mL/min). [9] [10] This also suggests that other components within the water, such as nitrates, sulfides, and heavy metals, do not impact the adsorption of phosphates to a significant degree as adsorption in water containing these components were similar to that of the synthetic wastewater. Additionally, it is important to highlight the fact that a slower flow rate would be acceptable, however altering the pH to a lower value would prove detrimental to aquatic ecosystems. An ideal compromise would involve a combination of lower flow rate and an increased quantity of CMNPs added to the water.

3.2 POSSIBLE MECHANISM FOR PHOSPHATE ADSORPTION

A possible mechanism for the adsorption of phosphate involves crosslinking with other components. [12] Figure 1 demonstrates a proposed phosphate adsorption mechanism due to chitosan's two excellent functional groups; $-NH_2$ and -OH. These functional groups provide the ability to combine with various compounds to treat wastewater. [20] It has been suggested that as the primary amine group becomes protonated in acidic conditions it binds to the metal oxide leaving the hydroxide group, as well as other protonated amine groups of the chitosan polymer with a partial positive charge allowing for electrostatic interactions with the negatively charged phosphate ions. [21] Since chitosan forms long chains of polymers, it has more than one adsorption site, which makes it an attractive method for adsorption. [22] During desorption with NaOH, the

phosphate groups lose their attraction to the now unprotonated amine groups and as a result further adsorption tests yield less phosphate adsorption.

Figure 1 demonstrates the proposed mechanism for phosphate adsorption using the protonated amine groups.

*Figure 1:* Possible Mechanism for Phosphate Adsorption
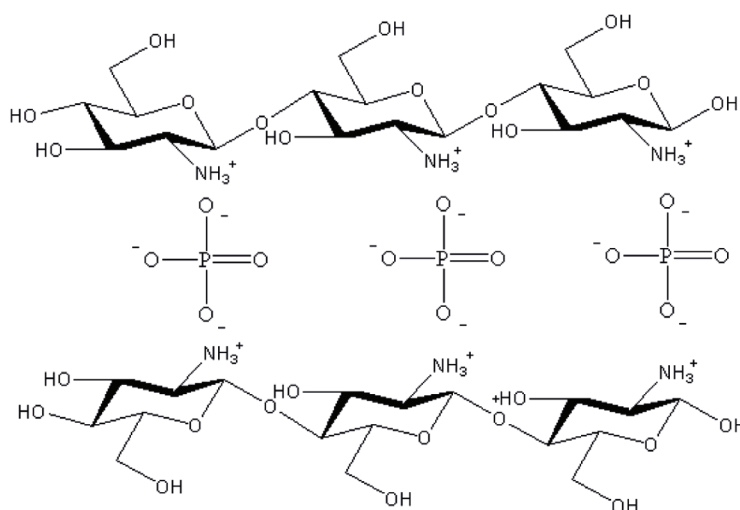
3.3 CHARACTERIZATION

3.3.1 Fourier-Transform Infrared Spectroscopy FTIR-ATR

Fourier-Transform Infrared Spectroscopy coupled with Attenuated Total Reflectance (FTIR-ATR) was utilized to determine the structure of the CMNPs which was taken before adsorption and after adsorption. Figure 2 demonstrates the differences in IR spectrums between pure chitosan and the CMNPs before and after adsorption. Pure chitosan shows peaks at 1014 cm^{-1} suggesting the vibration of a C-O-C bond. A peak at 1415 cm^{-1} demonstrates a deformation of the -CH bond bound to the -OH while a peak at 1543 cm^{-1} demonstrates the N-H bending of the amine group.

The spectra of CMNPs before adsorption indicated peaks at 3100-3400 cm^{-1} showing the presence of -OH stretching vibrations. The characteristic peak at 1546 cm^{-1} is more intense demonstrating N-H bending of the amine group as it is protonated. A peak at 1407 cm^{-1} which is also more intense,

Figure 2: FTIR-ATR of Pure Chitosan and CMNPs.
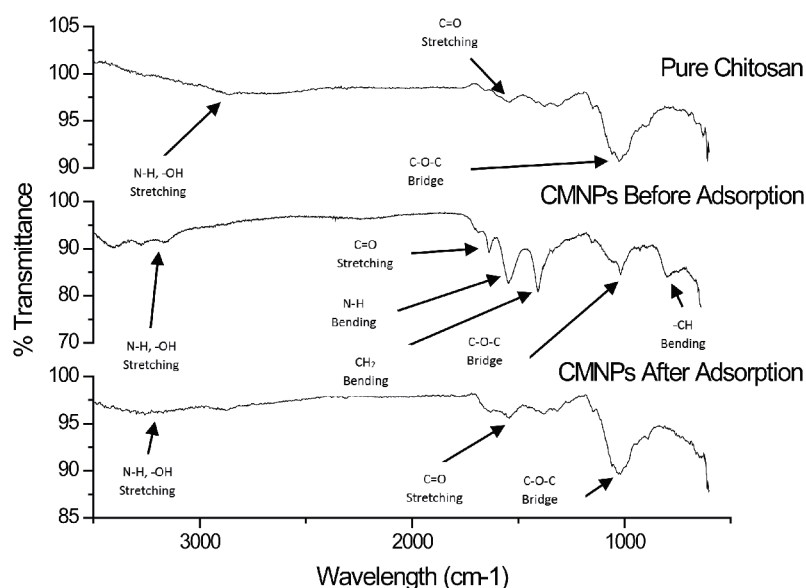
demonstrates a deformation of the -CH bond bound to the -OH which has a larger dipole moment. A slight peak at 1195 cm^{-1} suggests vibration of a C-O-C bond. [21] [23] A final peak at 810 cm^{-1} suggests the bending of a CH bond.

The spectra of CMNPs after adsorption is like that of pure chitosan. A peak at 1029 cm^{-1} suggests the vibration of a C-O-C bond indicating that the polymer is still present. A slight peak at 1381 cm^{-1} demonstrates a lower deformation of the -CH bond bound to the -OH while another slight peak at 1523 cm^{-1} demonstrates less N-H bending of the amine group.

3.3.2 Vibrating-Sample Magnetometer (VSM)

The magnetic strength of the synthesized nanoparticles was analyzed using a Vibrating-Sample Magnetometer (VSM) as shown in figure 3. The hysteresis curve of the synthesized nanoparticles demonstrated magnetic saturation values of 95 emu/g as the external magnetic field applied increases. This value demonstrates that the synthesized $Co_{80}Fe_{20}$ nanoparticles are superparamagnetic in their behavior with results comparable to those obtained by Chirac (2008) of 120 emu/g. The values also demonstrate that the synthesized nanoparticles will not be attracted to one another, but rather only present magnetic behavior in the presence of an external source. The similarity in results demonstrates that the methods used in synthesizing nanoparticles is replicable and reliable.

Figure 3: Magnetic strength using VSM
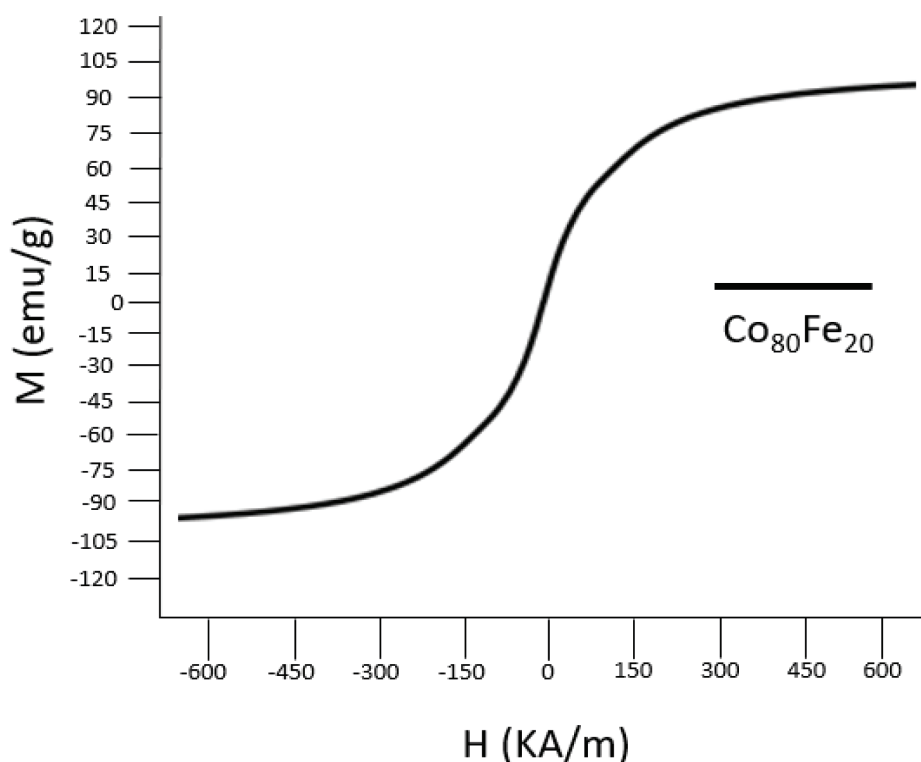
3.3.3 Scanning Electron Microscopy (SEM) and Transmission Electron Microscopy (TEM)

Scanning Electron Microscopy (SEM) and Transmission Electron Microscopy (TEM) was used to demonstrate the morphology of the nanoparticles, which were between 80 and 120nm in size and generally spherical in nature, as seen in Figure 4 and 5. Due to their size, the nanoparticles present a large surface area to volume ratio making them ideal for creating a complex with chitosan. Additionally, Energy-dispersive X-ray spectroscopy (EDS) was used to determine the composition and percent atomic mass of the nanoparticles synthesized in Figure 5 and is displayed in Figure 6. EDS analysis confirmed that the nanoparticles synthesized were composed of iron and cobalt. Carbon, sodium, and oxygen are expected due to being refluxed in ethylene glycol and using sodium hydroxide to raise the pH.

Figure 4*: TEM images of $Co_{80}Fe_{20}$ nanoparticles*
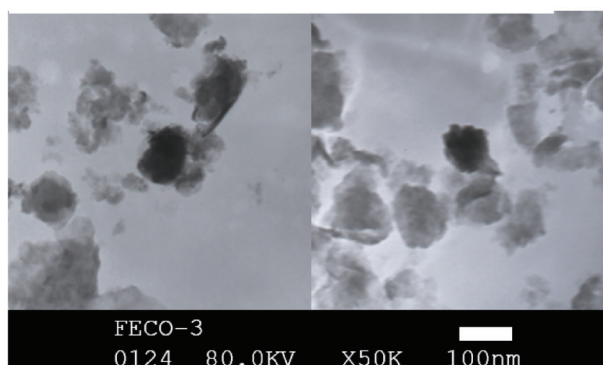
Figure 5*: SEM images of $Co_{80}Fe_{20}$*
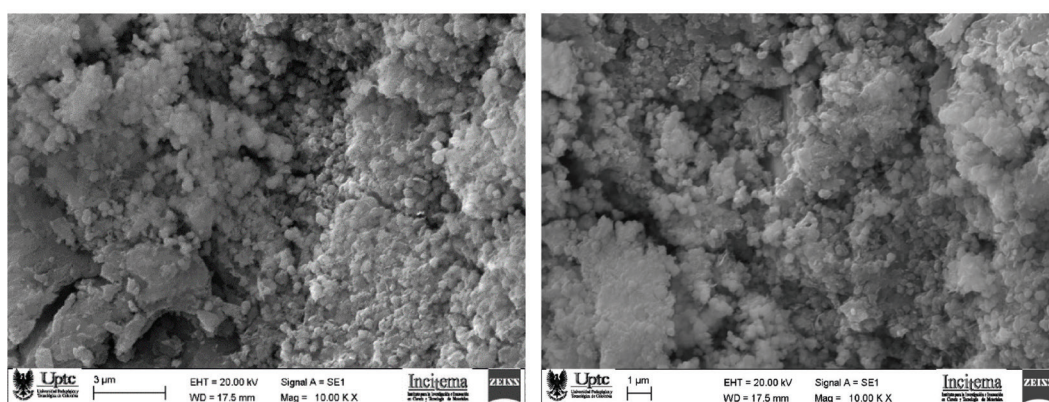
Figure 6: *EDS of Synthesized Nanoparticles*

Element	Atomic %
C	22.11
O	62.67
Na	5.11
Si	1.43
S	0.62
Fe	1.81
Co	6.26
Totals	100
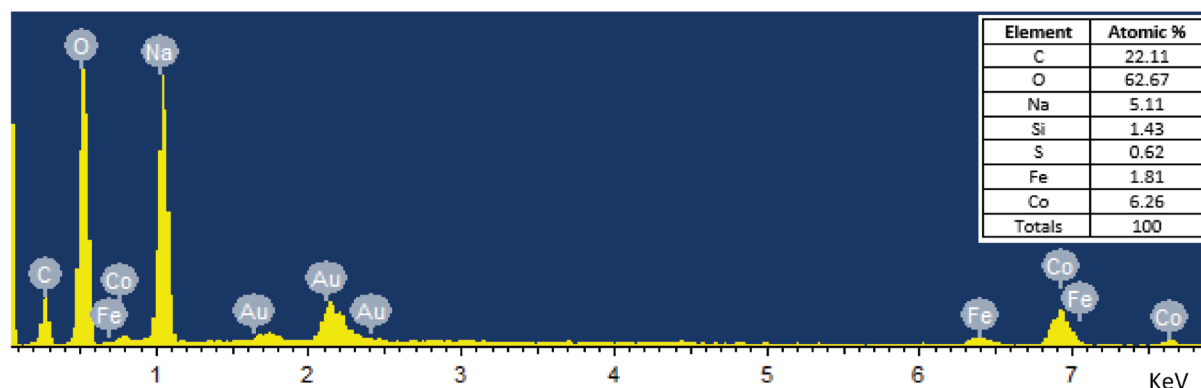
3.3.4 X-Ray Diffraction (XRD)

X-Ray Diffraction (XRD) was used to confirm the presence of iron and cobalt in the nanoparticles (Figure 7), as well as when modified with chitosan (Figure 8). This is due to the comparison from the diffractogram with those of the JCPDS cards. Results from the XRD analysis of Figure 7 showed that pure iron and cobalt nanoparticles were not formed but were rather oxidized to form iron oxide and cobalt oxide. Magnetite and hematite were found to be the main components within the iron-cobalt powder. Characteristic peaks typical of iron oxide were found at 31.17°, 35.12°, 41.38°, 52.38°, 57.22°, and 62.00° Bragg angle which correspond to the various crystal planes of iron oxide such as (220), (311), (400), (422), (511), and (440) as referenced with JCPDS card no 19-629. Characteristic peaks typical of cobalt oxide were found at 22.49°, 35.12°, 44.19°, 52.60°, 70.15°, and 77.26° which correspond to the various crystal planes of cobalt oxide such as (111), (220), (311), (400), (511), and (440) as referenced with JCPDS

Figure 7: Analysis Co$_{80}$Fe$_{20}$
nanoparticles using XRD.

Figure 8: Analysis of CMNPs
using XRD.
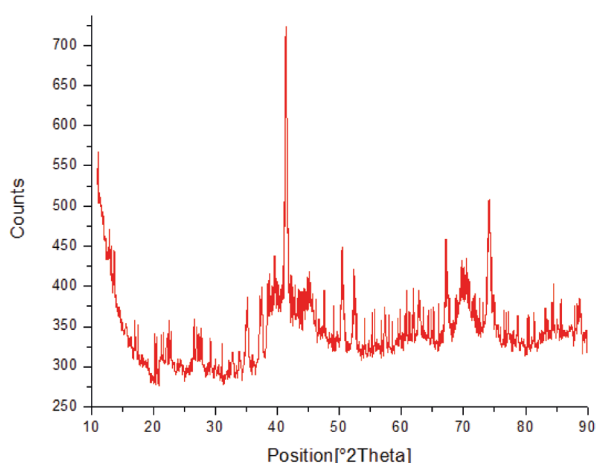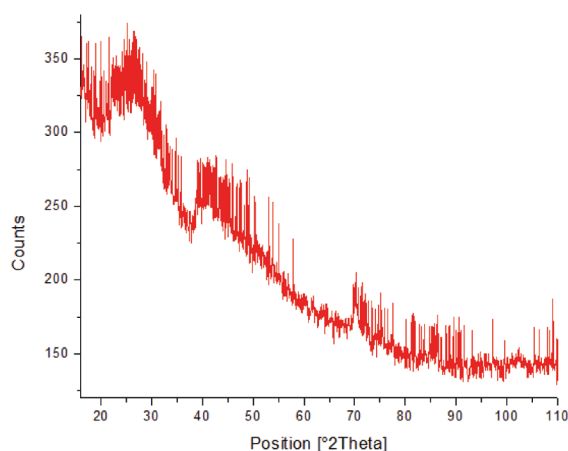

card no. 73-1701. The CMNPs were also examined in Figure 8 whose diffractogram closely resembled literature values recorded using XRD. [24] [25]

The broad nature of the peaks in Figure 8 was the result of the amorphous nature of the product.

3.3.5 Adsorption Isotherm Model

Adsorption isotherms were constructed from the experimental data obtained using the different equilibrium concentrations and analyzed using the Langmuir isotherm model. [26] The graph on the right side of Figure 9 demonstrates that time significantly impacts the amount of phosphate

adsorbed by the CMNPs. Within the first 15 minutes, approximately 98% of the phosphate in the water had been adsorbed. The graph on the left side of Figure 9 also demonstrates that the Langmuir isotherm model of adsorption capacity for this particular study as 0.138 mg/g of adsorbent. This particular isotherm presents an R^2 value of 0.983

Figure 9: Langmuir isotherm model of adsorption capacity (left) and adsorption-time isotherm (right) utilizing 0.5g of CMNPs for each test.
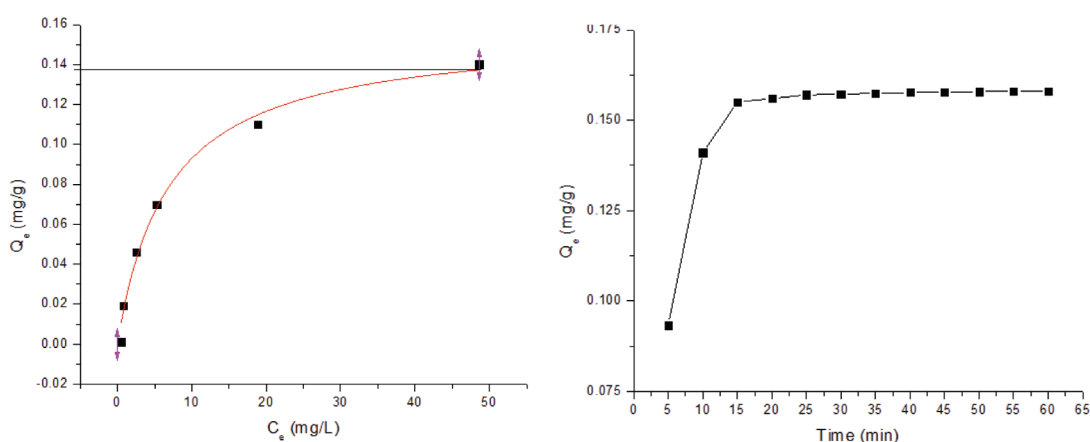
which suggests that the model is a good fit to the experimental data. Although the adsorption capacity is lower than other similar studies such as 26.5 by Hualin, 36.1 by Huang, 27.15 by Vicente, and 32.73 by Kumar. [10] [16] [17] [25] This was

attributed to using CMNPs in a gel state with a high water content thus lowering the adsorbent capacity per gram of adsorbent or Q_e. [9] [16]. However, this material could be considered as a better absorbent than typical biosorbents [27].

4. CONCLUSION

CMNPs were synthesized in order to determine their ability to adsorb phosphates from synthesized water, as well as natural river water, in a more realistic setting. Temperature, pH, and phosphate concentrations were maintained while the amount of CMNPs, flow rate, and desorption time were adjusted. Results indicated that the CMNPs were able to adsorb phosphates in both synthesized water and natural river water at similar levels. The results also confirmed that adsorption could take place with the presence of a flow of water instead of a simple batch adsorption highlighted in Table 2. The adsorption capacity isotherms demonstrated that peak adsorption capacity was found to be 0.138mg of phosphate per gram of adsorbent. Maximum adsorption was reached within approximately 15 min indicating that the adsorption process is relatively quick especially without altering pH or temperature. Repetitive adsorption/desorption cycles also add credibility to the ability of CMNPs to be utilized in wastewater treatment plants as shown by the various adsorption and desorption cycles in Table 2.

A benefit to the implementation of CMNPs in a wastewater treatment plant is that it would not require the alteration of pH or temperature. This would help to reduce costs and allows its implementation without having a negative impact on ecosystems and wildlife. Since chitosan is a biodegradable polymer its adsorption with phosphate may provide a unique use as a controlled-release fertilizer for crops. Although, tests were performed on a laboratory scale, the scaling up of the process may be possible. Two areas of further research are possible; the first being the efficiency of nitrate removal by CMNPs and the second being the efficiency of CMNPs separation from water. These studies would further cement chitosan's ability to be used in real-world applications to treat eutrophication.

DISCLOSURE STATEMENT

There is no conflict of interest nor any financial interest as a result of this study.

REFERENCES

[1] I. L. Pepper, G. C. P., and M. L. Brusseau, Environmental and Pollution Science 2nd Edition. Elsevier Inc., 2006.

[2] G. J. Tortora and B. H. Derrickson, Principles of Anatomy and Physiology 12th Edition. Hoboken, New Jersey: John Wiley & Sons Inc., 2009.

[3] J. O. Drangert, "Phosphorus - A limited resource that could be made limitless," Procedia Eng., vol. 46, pp. 228–233, 2012, doi: 10.1016/j.proeng.2012.09.469.

[4] D. Wasley, "Phosphorus: Sources, Forms, Impact on Water Quality - A General Overview," Minnesota, 2007.

[5] M. F. Chislock, E. Doster, R. Zitomer, and A. E. Wilson, "Eutrophication: Causes, consequences, and controls in aquatic ecosystems," Nat. Educ. Knowl., vol. 4, pp. 1–8, Jan. 2013.

[6] K. Campbell, "The Effects of Sewage on Aquatic Ecosystems," 2008. .

[7] M. Meybeck, "Carbon, nitrogen, and phosphorus transport by world rivers," Am. J. Sci., vol. 282, no. 4, pp. 401–450, 1982, doi: 10.2475/ajs.282.4.401.

[8] Corpoboyaca, "Diagnostico del plan de ordenamiento hídrico- PORH de la cuenca media y alta del rio chicamocha," Tunja, 2015.

[9] J. H. Kim, S. B. Kim, S. H. Lee, and J. W. Choi, "Laboratory and pilot-scale field experiments for application of iron oxide nanoparticle-loaded chitosan composites to phosphate removal from natural water," Environ. Technol. (United Kingdom), vol. 39, no. 6, pp. 770–779, 2018, doi: 10.1080/09593330.2017.1310937.

[10] H. Jiang, P. Chen, S. Luo, X. Tu, Q. Cao, and M. Shu, "Synthesis of novel nanocomposite Fe3O4/ZrO2/chitosan and its application for removal of nitrate and phosphate," Appl. Surf. Sci., vol. 284, pp. 942–949, 2013, doi: https://doi.org/10.1016/j.apsusc.2013.04.013.

[11] D. Liu, P. Wang, G. Wei, W. Dong, and F. Hui, "Removal of algal blooms from freshwater by the coagulation-magnetic separation method," Environ. Sci. Pollut. Res., vol. 20, no. 1, pp. 60–65, 2013, doi: 10.1007/s11356-012-1052-4.

[12] P. Nechita, "Applications of Chitosan in Wastewater Treatment," in Biological Activities and Application of Marine Polysaccharides, 2017, pp. 209–228.

[13] H. Chiriac, A. E. Moga, and C. Gherasim, "Preparation and characterization of Co, Fe and Co-Fe magnetic nanoparticles," J. Optoelectron. Adv. Mater., vol. 10, pp. 3492–3496, Dec. 2008.

[14] A. M. Escobaro, L. R. Pizzio, and G. P. Romanelli, "Catalizadores Magnéticos Basados En Óxidos De Hierro: Síntesis, Propiedades Y Aplicaciones," Ciencia En Desarrollo, vol. 10, no. 1, pp. 79–101, 2018, doi: 10.19053/01217488.v10.n1.2019.8811.

[15] Á. P. Sánchez Cepeda, R. Vera Graziano, E. de J. Muñoz Prieto, E. Y. Gomez Pachón, M. J. Bernard Bernard, and A. Maciel Cerda, "Preparación y caracterización de membranas poliméricas electrohiladas de policaprolactona y quitosano para la liberación controlada de clorhidrato de tiamina," Ciencia En Desarrollo, vol. 7, no. 2, p. 133, 2016, doi: 10.19053/01217488.v7.n2.2016.4818.

[16] Y. Huang, X. Lee, M. Grattieri, F. Macazo, R. Cai, and S. Minteer, "A sustainable adsorbent for phosphate removal: modifying multi-walled carbon nanotubes with chitosan," J. Mater. Sci., vol. 53, no. 17, pp. 12641–12649, Sep. 2018, doi: 10.1007/s10853-018-2494-y.

[17] I. de Vicente, A. Merino-Martos, L. Cruz-Pizarro, and J. de Vicente, "On the use of magnetic nano and microparticles for lake restoration," J. Hazard. Mater., vol. 181, no. 1–3, pp. 375–381, 2010, doi: 10.1016/j.jhazmat.2010.05.020.

[18] L. S. Clesceri et al., Standard Methods for the Examination of Water and Wastewater, no. v. 20. American Public Health Association, 1998.

[19] I. Langmuir, "The constitution and fundamental properties of solids and liquids," J. Am. Chem. Soc., vol. 38, no. 11, pp. 2221–2295, Nov. 1916, doi: 10.1021/ja02268a002.

[20] Z. Ali, "Extraction and Characterization of Chitosan from Indian Prawn (Fenneropenaeus Indicus) and its Applications on Waste Water Treatment of Local Ghee Industry,"

IOSR J. Eng., vol. 3, pp. 28–37, Oct. 2013, doi: 10.9790/3021-031022837.

[21] S. Hong, Y. Chang, and I. Rhee, "Chitosan-Coated Ferrite (Fe3O4) Nanoparticles as a T2 Contrast Agent for Magnetic Resonance Imaging," J. Korean Phys. Soc., vol. 56, no. 3, pp. 868–873, Mar. 2010, doi: 10.3938/jkps.56.868.

[22] F. Croisier and C. Jérôme, "Chitosan-based biomaterials for tissue engineering," Eur. Polym. J., vol. 49, no. 4, pp. 780–792, 2013, doi: 10.1016/j.eurpolymj.2012.12.009.

[23] S. Yasmeen, M. Kabiraz, B. Saha, M. Qadir, M. Gafur, and S. Masum, "Chromium (VI) Ions Removal from Tannery Effluent using Chitosan-Microcrystalline Cellulose Composite as Adsorbent," Int. Res. J. Pure Appl. Chem., vol. 10, no. 4, pp. 1–14, 2016, doi: 10.9734/irjpac/2016/23315.

[24] S. Logpriya et al., "Preparation and characterization of ascorbic acid-mediated chitosan–copper oxide nanocomposite for antimicrobial, sporicidal and biofilm-inhibitory activity," J. Nanostructure Chem., vol. 8, no. 3, pp. 301–309, 2018, doi: 10.1007/s40097-018-0273-6.

[25] I. A. Kumar and N. Viswanathan, "A facile synthesis of magnetic particles sprayed gelatin embedded hydrotalcite composite for effective phosphate sorption," J. Environ. Chem. Eng., vol. 6, no. 1, pp. 208–217, 2018, doi: 10.1016/j.jece.2017.11.042.

[26] X. Chen, "Modeling of experimental adsorption isotherm data," Information, vol. 6, no. 1, pp. 14–22, 2015, doi: 10.3390/info6010014.

[27] C. Tejada, A. Herrera, and E. Ruiz, "Utilización de biosorbentes para la remoción de níquel y plomo en sistemas binarios," Ciencia En Desarrollo, vol. 7, no. 1, pp. 31–36, 2016, doi: 10.19053/01217488.4228.

[28] A. Funes, J. de Vicente, and I. de Vicente, "Synthesis and characterization of magnetic chitosan microspheres as low-density and low-biotoxicity adsorbents for lake restoration," Chemosphere, vol. 171, pp. 571–579, 2017, doi: 10.1016/j.chemosphere.2016.12.101.

[29] H. M. F. Freundlich, "Over the Adsorption in Solution," J. Phys. Chem., vol. 57, pp. 385–471, 1906..